Hepatobiliary & Pancreatic Diseases International 18 (2019) 266–272

Contents lists available at ScienceDirect

Hepatobiliary & Pancreatic Diseases International

journal homepage: www.elsevier.com/locate/hbpd

Original Article/Liver

Au@SiO_2@$CuInS_2$–ZnS/Anti-AFP fluorescent probe improves HCC cell labeling

Yi-Wen Dai[a], Li-Xin Zhu[b], Yan Zhang[b], Shu-Hui Wang[c], Kui Chen[c], Tong-Tong Jiang[d], Xiao-Liang Xu[c], Xiao-Ping Geng[a,*]

[a] *Division of General Surgery, The Second Affiliated Hospital of Anhui Medical University, Hefei 230601, China*
[b] *Division of General Surgery, The First Affiliated Hospital of Anhui Medical University, Hefei 230022, China*
[c] *Key Laboratory of Strongly-Coupled Quantum Matter Physics, Chinese Academy of Sciences, School of Physical Sciences, University of Science and Technology of China, Hefei 230026, China*
[d] *Department of Physics, Anhui University, Hefei 230020, China*

ARTICLE INFO

Article history:
Received 28 October 2018
Accepted 28 February 2019
Available online 5 March 2019

Keywords:
Plasmon enhancement
Quantum dots
Nanoparticle
Luminescence
Cytotoxicity

ABSTRACT

Background: Clear tumor imaging is essential to the resection of hepatocellular carcinoma (HCC). This study aimed to create a novel biological probe to improve the HCC imaging.

Methods: Au nano-flower particles and $CuInS_2$–ZnS core-shell quantum dots were synthesized by hydrothermal method. Au was coated with porous SiO_2 and combined with anti-AFP antibody. HCC cell line HepG2 was used to evaluate the targeting efficacy of the probe, while flow cytometry and MTT assay were used to detect the cytotoxicity and bio-compatibility of the probe. Probes were subcutaneously injected to nude mice to explore light intensity and tissue penetration.

Results: The fluorescence stability of the probe was maintained 100% for 24 h, and the brightness value was 4 times stronger than that of the corresponding $CuInS_2$–ZnS quantum dot. In the targeting experiment, the labeled HepG2 emitted yellow fluorescence. In the cytotoxicity experiments, MTT and flow cytometry results showed that the bio-compatibility of the probe was fine, the inhibition rate of HepG2 cell with 60% Cu-QDs/Anti-AFP probe and Au-QDs/Anti-AFP probe solution for 48 h were significantly different (86.3%±7.0% *vs.* 4.9%±1.3%, $t = 19.745$, $P<0.05$), and the apoptosis rates were 83.3%±5.1% *vs.* 4.4%±0.8% ($P<0.001$). In the animal experiment, the luminescence of the novel probe can penetrate the abdominal tissues of a mouse, stronger than that of $CuInS_2$–ZnS quantum dot.

Conclusions: The Au@SiO_2@$CuInS_2$–ZnS/Anti-AFP probe can targetedly recognize and label HepG2 cells with good bio-compatibility and no toxicity, and the strong tissue penetrability of luminescence may be helpful to surgeons.

Introduction

Hepatocellular carcinoma (HCC) is a life threatening disease, ranking sixth of common malignant diseases and the second cause of cancer death. HCC in China accounts for about half of the world's new cases and mortalities [1,2]. HCC diagnosis is mainly relied on imaging and tumor markers, such as ultrasound, CT, MRI and alpha-fetoprotein (AFP). However, traditional imaging can only identify tumors with a certain diameter, tiny or even cell-level tumors can hardly be identified and imaged. Clearer and more precise imaging that detects the location and size of tumor is essential to plan tumor resection. Therefore, some researchers use organic fluorescent dyes for HCC imaging during surgery [3–5].

Quantum dots (QDs) is a hypotoxic semiconductor nanocrystal, which can emit different colors of fluorescence for a long time under the excitation of ultraviolet near infrared light. Compared to organic fluorescent dyes, QDs have a unique set of properties in terms of optics: (1) the wavelength of the excitation light changes are the same size of the QDs changes; (2) the QDs excitation wavelength range is wider, the emission wavelength range is narrower, and the fluorescence brightness is stronger; (3) the QDs can be linked to an targeted antibody by chemical modification. QDs probe has broad application in medical imaging [6–8].

Our previous studies [9,10] demonstrated that following the increases of the elements and complexity of QDs, the toxicity of the QDs was gradually decreased. Due to the weak absorption

* Corresponding author.
E-mail address: xp_geng@163.net (X.-P. Geng).

https://doi.org/10.1016/j.hbpd.2019.03.001
1499-3872/

of near-infrared light by body fluids and tissues, the complex of QDs-antibody may be used to detect internal organ tumors [11,12]. However, since the luminescence intensity of near-infrared QDs is weaker than that of visible light QDs [13–15], it is still difficult to fully and accurately reflect the size, depth and boundary of tumors when used as fluorescent markers for deep organs.

In this study, we synthesized a novel biological probe, Au@SiO_2@$CuInS_2$–ZnS/Anti-AFP probe. We used this complex to label HepG2 and evaluated the cytotoxicity, fluorescence brightness and tissue penetrability of the probe.

Methods

Materials

Reagents were purchased from Sigma Aldrich (St. Louis, MO, USA) or Gibco (New York, NY, USA). Cell line HepG2 was purchased from Cell Bank of Chinese Academy of Science, Shanghai, China, rabbit anti-AFP antibody from Proteintech Group, Wuhan, China, Annexin V-PI kit from BestBio, Shanghai, China, and BALB/c mouse from GemPharmatech, Nanjing, China. Flow cytometer was purchased from Beckman Coulter, California, USA, *in vivo* imaging system from Bio-Real, Salzburg, Austria, microplate reader (ELX 800) from Bio-Tek, Winooski, USA and Laser scanning Confocal Microscope from Leica, Wetzlar, Germany.

Synthesis of $CuInS_2$–ZnS QDs (Cu-QDs)

$CuInS_2$–ZnS QDs synthesis protocol was the same with previous study [16]. Briefly, the $CuInS_2$–ZnS core-shell QDs were prepared by adding 0.8 mmol $Zn(OAc)_2$•$2H_2O$, 1 mmol sodium citrate and 1.2 mmol glutathione into the $CuInS_2$ QD solution. Then 0.8 mmol Na_2S solution was slowly added. After stirring for 10 min, the reaction solution was heated for 2 h at 100 °C. The mixed solution was transferred into a 15 mL autoclave and heated at 150 °C for 21 h. After the solution was cooled to room temperature, ethanol was added. The precipitation was centrifuged with high-speed centrifuge (10 000 rpm, 3 min) and the pellet was dissolved in the deionized water.

Synthesis of Au@SiO_2@$CuInS_2$–ZnS QDs (Au-QDs)

There are 5 steps in the synthetic process. (1) Synthesis of Au nanospheres: 0.6 mL of $NaBH_4$ (10 mmol/L in ice bath was added to 10 mL of $HAuCl_4$ (0.25 mmol/L) and CTAB (0.1 mol/L) aqueous solution. The solution was incubated at 30 °C for 3 h; added 0.3 mL Au nanosphere and 5 mL Acrylic Acid (AA, 0.09 mol/L) to 12 mL of $HAuCl_4$ (0.25 mmol/L) and hexadecyl trimethyl ammonium bromide (CTAB, 0.1 mol/L). The mixture was centrifuged at 12 000 rpm for 45 min, and then the pellet was dissolved in 1 mL of pure water. (2) Polyvinyl pyrrolidone (PVP)-stabilized gold seed crystal: 200 μL of the prepared Au nanosphere solution was added to 6 mL of dimethyl formamide (DMF) solution containing $HAuCl_4$ (0.16 mmol/L) and PVP (Mw=10,000, 0.21 mol/L), and then, the reaction solution was stirred for 1 h in an oil bath at 80 °C. (3) Synthetic gold nanoflowers: 15 mL of PVP (0.4, 0.6 and 0.9 mol/L, respectively) and 180 μL of $HAuCl_4$ were mixed. The Au seed crystals were added and stirred for 2 h. The obtained product was washed twice and dissolved in alcohol. (4) Preparation of Au nanoflowers @SiO_2: 3 mL of water was added to the alcohol solution of Au nanoflowers, and 1 mL of ammonia water was introduced. Then 15 μL, 20 μL and 80 μL of a mixture of ammonium persulfate (APS) and tetraethylorthosilicate (TEOS) (molar ratio of 2:1) were added under vigorous stirring for 20 min, and the product was washed with alcohol and finally dissolved in pure water. (5) Preparation of Au nanoflowers@SiO_2@$CuInS_2$–ZnS QDs: 100 μL of QDs were added to Au nanoflowers@SiO_2 aqueous solution. After 10 min of ultrasound, the product was centrifuged and dissolved in phosphate buffer saline (PBS).

Preparation of Au@SiO_2@$CuInS_2$–ZnS/Anti-AFP and $CuInS_2$–ZnS/Anti-AFP probe

UV–visible absorbance was measured using a UV-3600 UV-VIS-NI spectrophotometer. Photoluminescence spectra were measured by using F-4600 fluorescence spectrophotometer. Twenty mL of APS was added into Au@SiO_2@$CuInS_2$–ZnS QDs and $CuInS_2$–ZnS QDs composite nanomaterial respectively, and incubated for 6 h at room temperature. Both were centrifuged and dispersed in PBS buffer. Ten mg of APS-modified composite nanoparticles were dissolved in 1 mL of PBS (containing 5% formaldehyde), incubated for 2 h in a shaker, centrifuged and dispersed in PBS buffer, and 100 μL of anti-AFP antibody (concentration: 1 mg/mL) was added to the above solution for 4 h, and finally the solution was washed three times with PBS buffer to obtain Au@SiO_2@$CuInS_2$–ZnS/Anti-AFP probe (Au-QDs/Anti-AFP probe) and $CuInS_2$–ZnS/Anti-AFP probe (Cu-QDs/Anti-AFP probe), and stored at 4 °C.

Cell labeling and imaging

HepG2 cells were cultured with medium (90% DMEM, 10% FBS, 1% Penicillin-Streptomycin) and fixed on the slides, and 50 μL Au-QDs/Anti-AFP probe and 50 μL Au-QDs solution (0.24 mg/mL) were dropped onto the slides, respectively, and incubated at 37 °C for 40 min, then PBS washed 3 times to remove free probes. After dyed with 4′,6-diamidino-2-phenylindole (DAPI), laser scanning confocal microscope was used for analysis. Yellow fluorescence from QDs and blue fluorescence from DAPI can be excited by light at the wavelength of 520 nm and 360 nm, respectively.

MTT assay

The 100 μL suspension cells ($5–10 \times 10^4$/mL) were planted into 96-well plates, and the medium was discarded when the cells were fully attached. Different concentrations (2.5%, 5%, 10%, 20%, 40%, and 60%) of Au-QDs/Anti-AFP probe (experiment) and Cu-QDs/Anti-AFP probe (control) in 100 μL medium were added into these wells, with each concentration tested in 5 wells. And then, three 96-well plates were cultured at 37 °C for 12, 24, and 48 h, respectively. After the 150 μL dimethyl sulfoxide (DMSO) was added and all the plates were shaken for 10 min in dark, and the optical density (OD) value was read with a plate reader at 490 nm to calculate the cell survival rate which equal to (E-Z)/(C-Z) × 100% (E, C, Z were OD value of experimental group, control and zero setting group, respectively).

Flow cytometry

Exponential phase HepG2 cells with $5–10 \times 10^5$/well were cultured in 6-well plates with 2 mL medium contains 60% of Au-QDs/Anti-AFP probe or Cu-QDs/Anti-AFP probe solution, and blank control group was cultured in medium without probe. After 48 h of incubation, AnnexinV-PI kit was used to detect the cell apoptosis with a flow cytometer.

Animal experiment

Six-week-old BALB/c mice were used in this study. Au@SiO_2@$CuInS_2$–ZnS/Anti-AFP probe (0.2 mL) or $CuInS_2$–ZnS/Anti-AFP probe (0.2 mL) was injected into different site (shoulder, quarter ribs and partes iliaca). Two minutes later, the fluorescence emitted from the mice was detected with Bio-Real *in vivo* imaging system.

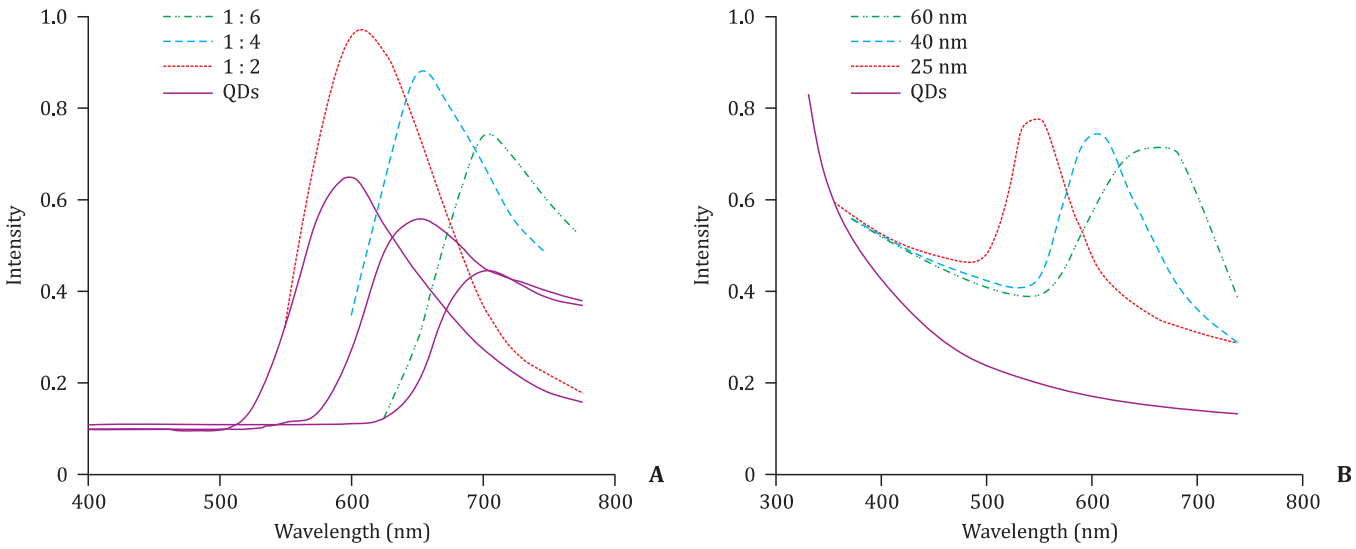

Fig. 1. A: Photoluminescence spectra (excitation wavelength EX=365 nm for QDs, and EX=550 nm, 600 nm, 620 nm for the three Au-QD/Anti-AFP probes, respectively) of $CuInS_2$–ZnS QDs (QDs, solid line) and Au–$CuInS_2$–ZnS (Au-QD, dashed lines), wherein the ratio of In:Cu is 1:2, 1:4 and 1:6 when preparing QDs (the corresponding QDs PL are three solid curves from left to right, respectively); **B**: corresponding absorption spectra: where the solid line is the QDs absorption spectrum and the dashed lines are the absorption spectra of the gold nanoflowers (linking QDs) with different diameters. QD: quantum dot.

Statistical analysis

Data that conform to normal distribution were expressed as mean ± SD, and were analyzed using SPSS 22.0. ANOVA (one-way) were used to analyze the time and dose effects. A P value of <0.05 was considered statistically significant.

Results

Optical property of Au-QDs/Anti-AFP probe

The different In:Cu ratios at the time of preparation of QDs caused the photoluminescence spectroscopy emission peaks of QDs, and the ratio of In:Cu is 1:2, 1:4 and 1:6, respectively (Fig. 1A). The emission peaks were 590 nm (600 nm), 630 nm (643 nm) and 690 nm (705 nm) (corresponding to the composite probe emission peak position in parentheses). The emission of the nanocomposite probe had a certain degree of red shift relative to the purity spectrum of QDs, because the composite probe was coated with SiO_2 which had caused the refractive index of the probe to become larger. From the area covered by the spectral coverage, the emission intensity of the composite probe was higher than that of the QDs, due to the resonance enhancement effect of plasmon on excitation light [17] and the acceleration of QDs fluorescence radiation [18]. The absorption spectrum of different QDs changed little, and one of the curves was shown in Fig. 1B. However, the absorption spectrum of gold nanoflowers had a significant red shift with its diameter. The absorption peaks of 25 nm, 40 nm and 60 nm gold nanoflowers were 550 nm, 605 nm and 664 nm, respectively.

The absorption spectrum of the gold nanoflower-QDs composite probe was a superposition of the QDs and the gold absorption spectrum. Since the absorption peak of gold got closer to the near-infrared region, the disadvantage of QD absorbed weakly near the near-infrared was avoided, as shown in Fig. 1B. It can be seen that the absorption of the Au-QD/Anti-AFP probe was stronger than that of the QD from several peak ranges of 550 nm to 700 nm. Therefore, in the *in vivo* body labeling experiment, near-infrared light with strong penetration into living tissue can be used as the excitation light source for the Au-QD/Anti-AFP probe labeling case. Fig. 1B showed the plasmon resonance absorption of three samples. As the size of nanoflower increased, their absorption peaks can be adjusted from visible to near-infrared. This phenomenon is due to that the surface plasmon resonance peak was closely related to the local electric field distribution of the metal nanoparticles. The charges were often localized at the sharp corners of the nanoparticles. The increased size resulted in the enhancement of the distance between positive and negative charges. This would increase the plasmon resilience, and cause the movement of the surface plasmon peak [19].

Representation of Au nanoflower structure

In order to study the effect of PVP solubility on the product absorption peak, three samples were synthesized. As the concentration of PVP decreased, the absorption peak of nanoflowers continuously violet shift approached the seed crystal. This should be due to a high proportion of vinylpyrrolidone monomer/Au atoms resulted in a fast, kinetically controlled growth phenomenon. Based on thermodynamics, the nanoparticles grew along the facets of low surface energy. The preferred growth process of the nanoparticles was inhibited because of the decrease of PVP concentration. This hindered the synthesis of dendritic nanostructures, resulted in the formation of spherical-like nanoparticles.

Fig. 2A was a 60 nm sample of three Au nanoflower samples with corresponding absorption peaks to the far right of Fig. 1B, and Fig. 2B was a structural representation of the Au-QDs/Anti-AFP probe. As the size of nanoflowers increased, their absorption peaks can be adjusted from visible to near-infrared because the distance between positive and negative charge resonances increased, resulted in additional energy loss [20] and the plasmon peak moved toward the infrared direction with less energy.

Cell labeling and imaging

In Au-QDs/Anti-AFP probe group (experiment), both the blue nuclei and the yellow fluorescent cytoplasm can be observed under the yellow-blue dual channel (Fig. 3A), while under the blue channel only blue nucleus can be observed (Fig. 3B). In Au-QDs group (control), under both blue channel and yellow-blue dual channel, only the blue nucleus can be observed (Fig. 3C and D). This experiment presented that the synthesized probes can target labeled

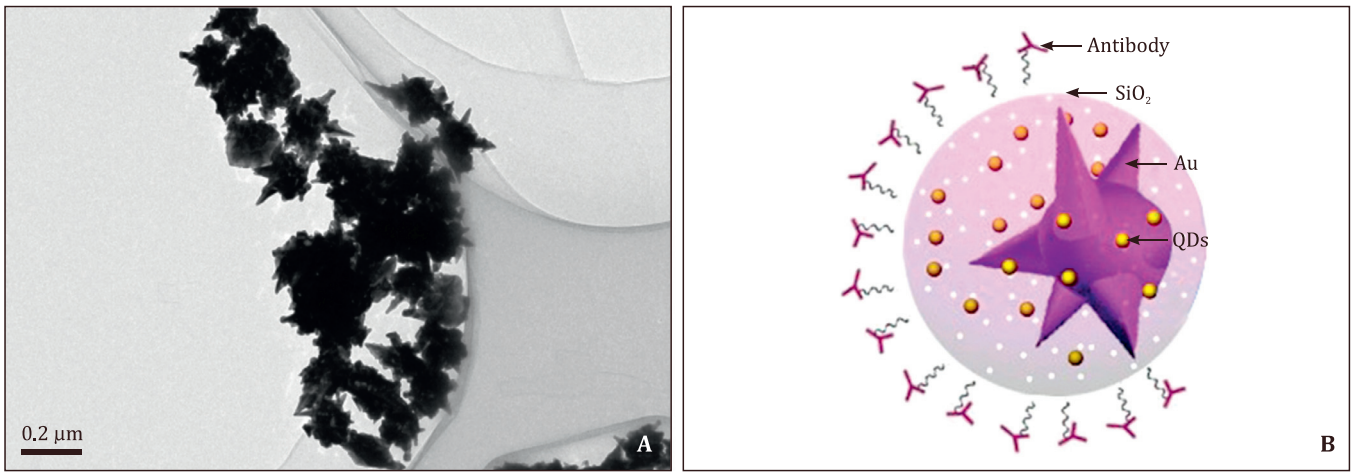

Fig. 2. **A**: The transmission electron microscopy (TEM) image of Au nanoflower structure (original magnification × 75,000); **B**: structural representation of the Au-QDs/Anti-AFP probe. QD: quantum dot.

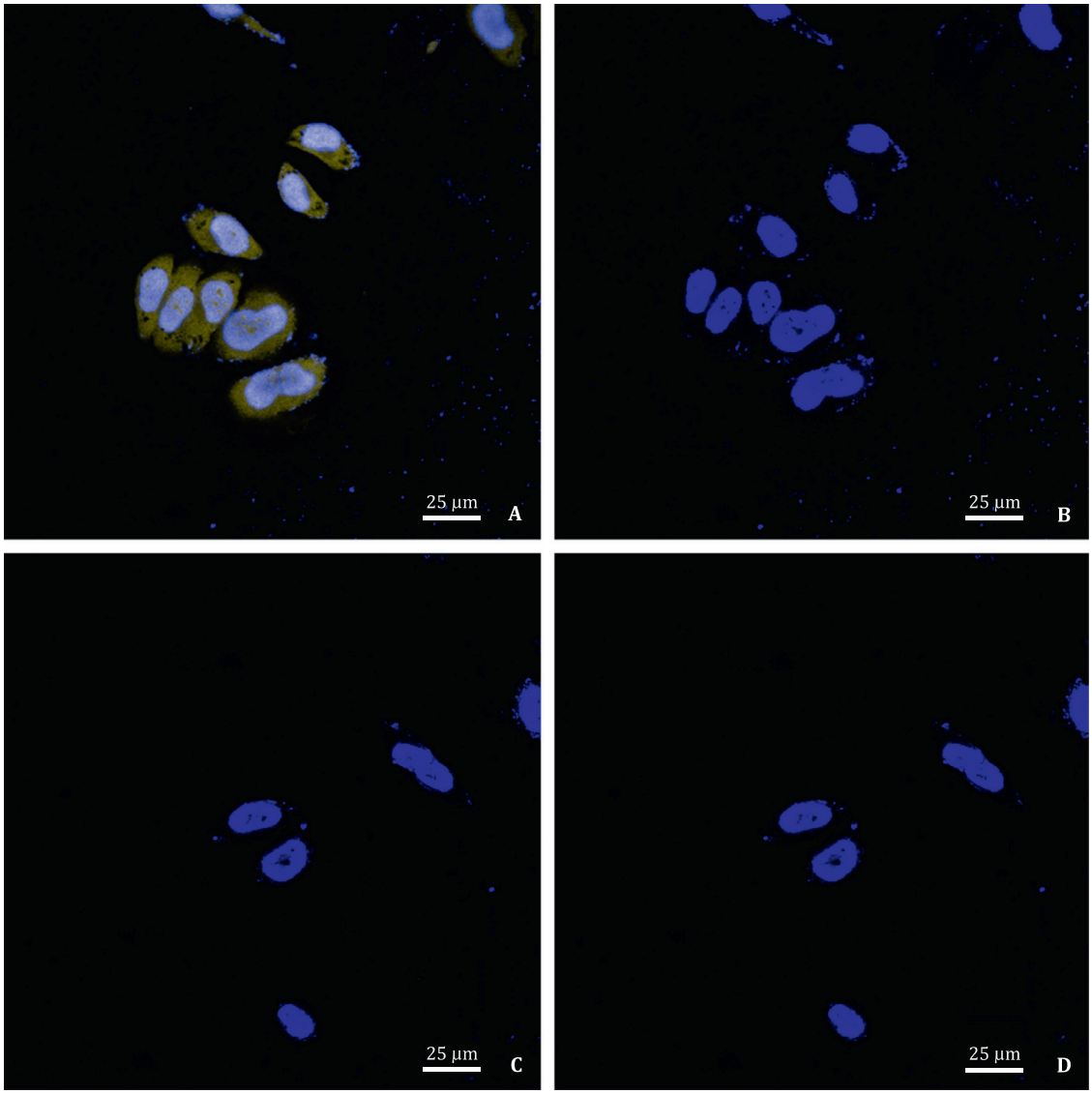

Fig. 3. **A**: Yellow–blue dual channel of the experimental group; **B**: blue channel of the experimental group; **C**: yellow–blue dual channel of the control group; **D**: blue channel of the control group. Original magnification × 600.

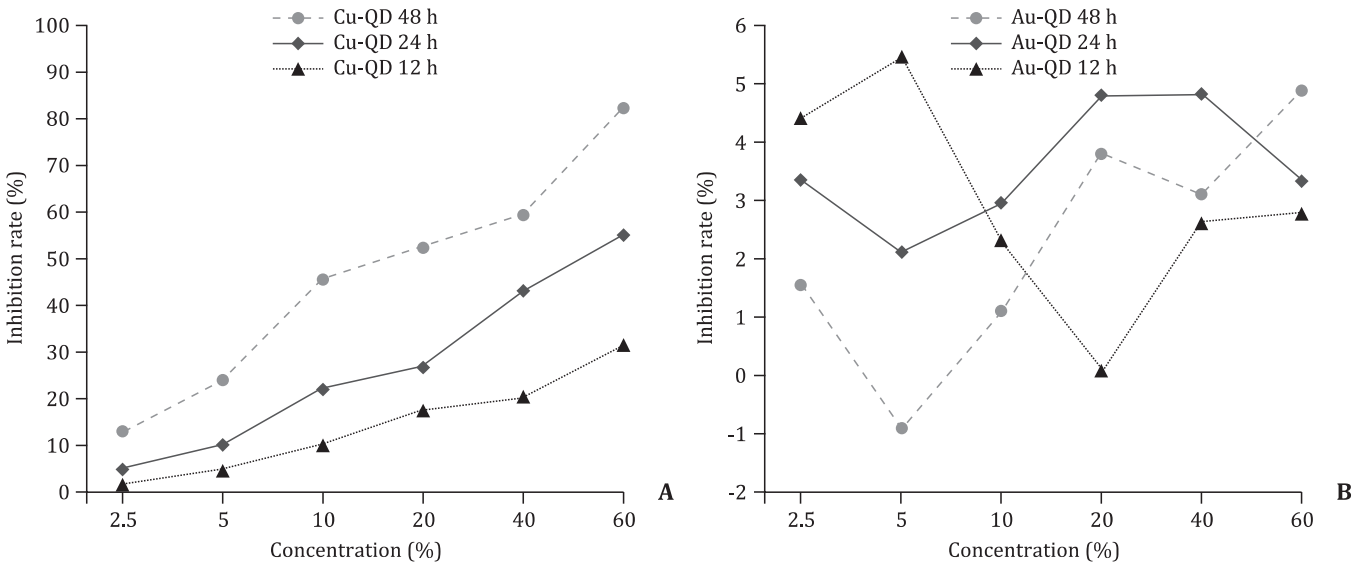

Fig. 4. The cell inhibition rate of Cu-QD/Anti-AFP probe (**A**) and Au-QD/Anti-AFP probe (**B**) were calculated and presented. QD: quantum dot.

cells through specific binding of antigen and antibody reaction and imaged the HCC cells through fluorescence emitted from QDs.

MTT assay

The inhibition rates of the probes were calculated and plotted as a line graph. In the Cu-QDs/Anti-AFP probe group, there was a positive correlation between the probe concentration and the inhibition rate at 12 h, 24 h, and 48 h, respectively ($P<0.05$, Fig. 4A).

In the Au-QDs/Anti-AFP probe group, there were no significant relation between the inhibition rate and the probe concentration and time of incubation ($P>0.05$, Fig. 4B). The inhibition rate of Cu-QDs/Anti-AFP probe and Au-QDs/Anti-AFP probe in 48h-60% were significantly different (86.3%±7.0% *vs.* 4.9%±1.3%, $t=19.745$, $P<0.05$). The cytotoxicity tests presented the fine biocompatibility of the Au-QDs/Anti-AFP probe.

Flow cytometry

The apoptosis rate of blank control group (Fig. 5A), Au-QDs/Anti-AFP probe group (Fig. 5B), and Cu-QDs/Anti-AFP probe group (Fig. 5C) was presented. ANOVA (one-way) showed that the mean apoptosis rate of the three groups were not equal ($F=670.146$, $P<0.001$). Multiple comparisons showed no significant difference between the blank control group and the Au-QDs/Anti-AFP probe group (3.8%±1.0% *vs.* 4.4%±0.8%, $P=0.878$), but the Cu-QDs/Anti-AFP probe group was statistically different from the blank control group (83.3%±5.1% *vs.* 3.8%±1.0%, $P<0.001$) and the Au-QDs/Anti-AFP probe group (83.3%±5.1% *vs.* 4.4%±0.8%, $P<0.001$) respectively (Fig. 5D). The apoptosis rate of Au-QDs/Anti-AFP probe was lower than 5%, indicating that the probe was not significantly toxic.

Animal experiment

The pseudo imaging of different probes in a mouse illuminated with infrared was presented in Fig. 6. The image was taken with a small animal fluorescence camera with an excitation wavelength of 620 nm. The selection of this excitation wavelength was based on the absorption spectra of two Au-QDs/Anti-AFP probe of In:Cu=1:4 and In:Cu=1:6. According to Fig. 1B, 620 nm was at the overlapping wavelength of two absorption peaks. It can be seen from the brightness comparison of the three regions in Fig. 6 that the brightness of region 2 and region 3 was stronger than the region 1 of the same QDs, because the plasmon resonance absorption effect of the Au nanoflowers at 620 nm was obtained. The absorption of the composite probe was stronger than that of the QDs, and the excitation rate of the Au-QDs/Anti-AFP probe fluorescence was faster than that of the QDs. The fluorescence intensity of region 3 was also brighter than region 2, because the fluorescence wavelength of region 2 was 705 nm, which was closer to the center of "near infrared window" of the living body, therefore, its transmittance was stronger than that of region 2 (643 nm).

Discussion

In our previous study [9], $CuInS_2$–ZnS–AFP core-shell QDs probe was synthesized to eliminate the majority of cytotoxicity of the ZnS shell. The coating of $CuInS_2$ QDs not only increases the QDs stability, but also effectively protects the inner core, greatly reducing the fluorescent bleaching effect caused by oxidation reaction, reducing its cytotoxicity.

In this study, Au@SiO_2@$CuInS_2$–ZnS QDs was synthesized, and the toxicity of QDs is completely eliminated with the package of SiO_2 on QDs and Au nanoflowers. The cytotoxicity of gold nanoparticles has been reported to be related to particle size and coagulation. When the particle size is greater than the threshold for endocytosis, the nanoparticles will adhere to the membrane surface rather than get into the cells [21]. The Au-QDs/Anti-AFP probe we prepared was less than 100 nm in diameter and therefore can enter the interior of the cell through the cell window. Since Au nanoflower and QDs were encapsulated by SiO_2 to form a protective film, the overall cytotoxicity of the Au-QDs/Anti-AFP probe was eliminated completely. Our MTT assay and flow cytometry showed that the Au-QDs/Anti-AFP probe had no cytotoxicity and fine biocompatibility.

The weak brightness and poor tissue penetration of QDs are caused by the following two reasons. Firstly, the fluorescence is greatly absorbed by body fluid and tissues in the process of penetrating. Secondly, although the absorption of near-infrared light (630–1100 nm wavelength) by the tissue is weaker, the body absorbs light 2–3 order of magnitudes weaker than the ultraviolet to visible region, thus near-infrared QDs are used to link the antibody frequently [22,23]. The absorption of light by near-infrared QDs is exponentially attenuated from the ultraviolet to the near-infrared wavelength. The result is that the excitation efficiency of

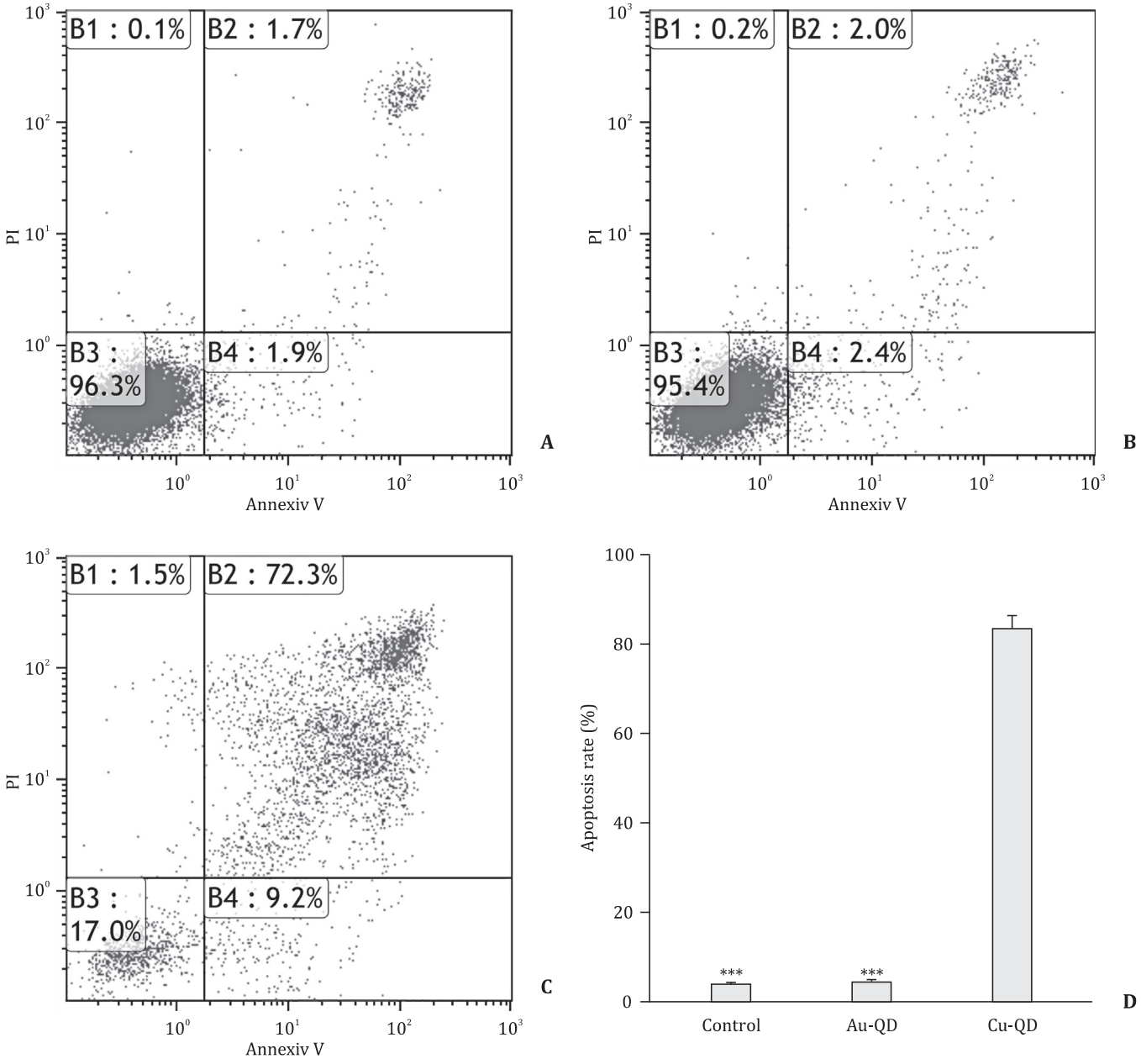

Fig. 5. The apoptosis rate was detected by flow cytometry. HepG2 cells were incubated with medium contains different probes for 48 h. **A**: Blank control medium with no probe; **B**: medium contains 60% of Au-QDs/Anti-AFP probe; **C**: medium contains 60% of Cu-QDs/Anti-AFP probe; **D**: mean apoptosis rate of three groups. ***: $P<0.001$, compared with the Cu-QDs/Anti-AFP probe group. QD: quantum dot.

the near-infrared light source is very low, and the luminous intensity is weaker than the visible QDs [14,15]. So the near-infrared QDs probe cannot be imaged clearly *in vivo*.

To resolve the problem, we designed and synthesized a novel plasmon fluorescence-enhanced probe based on gold nanoflower-QD/Antibody structure, which enhances the luminescence intensity greatly. The plasmon resonance absorption effect of Au nanoflowers was used to shift the excitation wavelength from the ultraviolet to the near-infrared region, and to enhance the luminescence intensity of the QDs more than 4 times of the general QDs.

Since the chemical reactivity of In^{3+} is stronger than that of Cu^{+}, the reaction between In^{3+} and S^{2-} is more complete than that of Cu^{+} and S^{2-} [24]. In $CuInS_2$, during the QD formation process, if the proportion of Cu^{+} is large (*i.e.*, In:Cu is reduced), unreacted Cu^{+} and S^{2-} vacancies are increased [25]. According to theoretical analysis, the Cu^{+} and S^{2-} vacancies in the gaps in the crystal are in the forbidden band of the band structure, and the S^{2-} vacancy level is higher than the Cu^{+} level. The main fluorescent peak is due to the electron–hole complexing between the sulfur vacancy level and the Cu^{+} level. With increasing Cu doping, the Cu^{+} level will increase in the forbidden gap [26,27], reducing the energy level difference between S^{2-} and Cu^{+} and causing a red shift in the main fluorescent peak.

The imaging of the animal experiment in this study presented that the fluorescence brightness of the probe from strong to weak were $Au@SiO_2@CuInS_2$–ZnS/Anti-AFP (In:Cu =1:6), $Au@SiO_2@CuInS_2$–ZnS/Anti-AFP (In:Cu =1:4) and $CuInS_2$–ZnS QD (In:Cu =1:4). It means that the novel probe can enhance the fluorescence brightness of the QDs, and the appropriate proportion of In to Cu can improve the brightness further. The brightness of

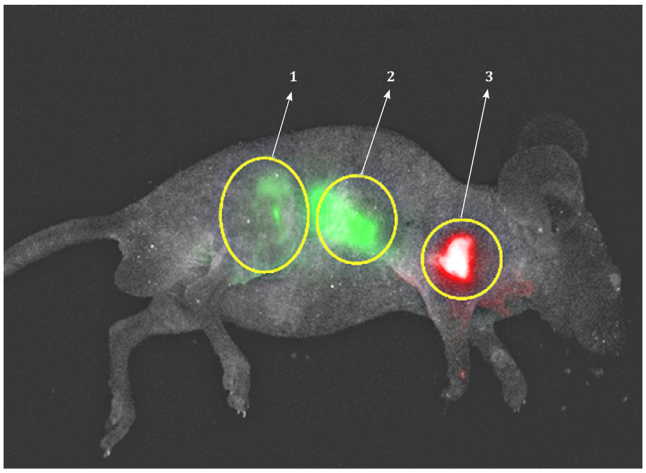

Fig. 6. Pseudo imaging of different QDs in a mouse illuminated with infrared. Region 1 (partes iliaca): $CuInS_2$–ZnS QD (In:Cu=1:4) with the emission wavelength of 630 nm; Region 2 (quarter ribs): Au@SiO_2@$CuInS_2$–ZnS/Anti-AFP (In:Cu=1:4) with the emission wavelength of 643 nm; Region 3 (shoulder): Au@SiO_2@$CuInS_2$–ZnS/Anti-AFP (In:Cu =1:6) with the emission wavelength of 705 nm.

the novel probe was enough to penetrate the abdominal tissues of a mouse.

With the problems of cytotoxicity and fluorescence brightness solved gradually, Au-QDs/Anti-AFP composite probe could be expected to be used in clinical practice.

Acknowledgments

We are grateful to Mr. Xue-Lin Cai and Mr. Da-Ke Huang for their generous help on flow cytometry and confocal microscopy.

Contributors

ZLX, XXL and GXP proposed the study. DYW, ZY, WSH and CK performed the research and wrote the first draft. JTT collected and analyzed the data. DYW and ZLX contributed equally to this article. All authors contributed to the design and interpretation of the study and to further drafts. GXP is the guarantor.

Funding

This research was supported by grants from the National Natural Science Foundation of China (51672003 and 51872279).

Ethical approval

This study was approved by the Experimental Animal Ethics Committee of Anhui Medical University (LLSC20170440).

Competing interest

No benefits in any form have been received or will be received from a commercial party related directly or indirectly to the subject of this article.

References

[1] Torre LA, Bray F, Siegel RL, Ferlay J, Lortet-Tieulent J, Jemal A. Global cancer statistics, 2012. CA Cancer J Clin 2015;65:87–108.
[2] Zuo TT, Zheng RS, Zhang SW, Zeng HM, Chen WQ. Incidence and mortality of liver cancer in China in 2011. Chin J Cancer 2015;34:508–513.
[3] Zhao YJ, Ju Q, Li GC. Tumor markers for hepatocellular carcinoma. Mol Clin Oncol 2013;1:593–598.
[4] Ariff B, Lloyd CR, Khan S, Shariff M, Thillainayagam AV, Bansi DS, et al. Imaging of liver cancer. World J Gastroenterol 2009;15:1289–1300.
[5] Kokudo N, Ishizawa T. Clinical application of fluorescence imaging of liver cancer using indocyanine green. Liver Cancer 2012;1:15–21.
[6] Liu D, Wang L, Ma S, Jiang Z, Yang B, Han X, et al. A novel electrochemiluminescent immunosensor based on CdS-coated ZnO nanorod arrays for HepG2 cell detection. Nanoscale 2015;7:3627–3633.
[7] Shi Y, Pramanik A, Tchounwou C, Pedraza F, Crouch RA, Chavva SR, et al. Multifunctional biocompatible graphene oxide quantum dots decorated magnetic nanoplatform for efficient capture and two-photon imaging of rare tumor cells. ACS Appl Mater Interfaces 2015;7:10935–10943.
[8] Shao D, Li J, Pan Y, Zhang X, Zheng X, Wang Z, et al. Noninvasive theranostic imaging of HSV-TK/GCV suicide gene therapy in liver cancer by folate-targeted quantum dot-based liposomes. Biomater Sci 2015;3:833–841.
[9] Yang MY, Hong J, Zhang Y, Gao Z, Jiang TT, Song J, et al. Bio-compatibility and cytotoxicity studies of water-soluble CuInS2–ZnS–AFP fluorescence probe in liver cancer cells. Hepatobiliary Pancreat Dis Int 2016;15:406–411.
[10] Song J, Ma C, Zhang W, Li X, Zhang W, Wu R, et al. Bandgap and structure engineering via cation exchange: from binary Ag2S to ternary AgInS2, quaternary AgZnInS alloy and AgZnInS/ZnS core/shell fluorescent nanocrystals for bioimaging. ACS Appl Mater Interfaces 2016;8:24826–24836.
[11] Ballou B, Lagerholm BC, Ernst LA, Bruchez MP, Waggoner AS. Noninvasive imaging of quantum dots in mice. Bioconjug Chem 2004;15:79–86.
[12] Choi HS, Liu W, Misra P, Tanaka E, Zimmer JP, Itty Ipe B, et al. Renal clearance of quantum dots. Nat Biotechnol 2007;25:1165–1170.
[13] Zheng X, Wang X, Mao H, Wu W, Liu B, Jiang X. Hypoxia-specific ultrasensitive detection of tumours and cancer cells *in vivo*. Nat Commun 2015;6:5834.
[14] Wada H, Hyun H, Vargas C, Gravier J, Park G, Gioux S, et al. Pancreas-targeted NIR fluorophores for dual-channel image-guided abdominal surgery. Theranostics 2015;5:1–11.
[15] Kamkaew A, Sun H, England CG, Cheng L, Liu Z, Cai W. Quantum dot-NanoLuc bioluminescence resonance energy transfer enables tumor imaging and lymph node mapping *in vivo*. Chem Commun (Camb) 2016;52:6997–7000.
[16] Jiang TT, Yin NQ, Liu L, Song J, Huang QP, Zhu LX, et al. Au nanoflower@SiO2@CdTe/CdS/ZnS quantumdot multi-functional nanoprobe for photothermal treatment and cellular imaging. RSC Adv 2014;4:23630–23636.
[17] Sugawa K, Tamura T, Tahara H, Yamaguchi D, Akiyama T, Otsuki J, et al. Metal-enhanced fluorescence platforms based on plasmonic ordered copper arrays: wavelength dependence of quenching and enhancement effects. ACS Nano 2013;7:9997–10010.
[18] Yuan L, Zhu J, Ren Y, Bai S. Sectional area-dependent plasmonic shifting in the truncated process of silver nanoparticles: from cube to octahedron. J Nanopart Res 2011;13:6305–6312.
[19] Sabaeian M, Khaledi-Nasab A. Size-dependent intersubband optical properties of dome-shaped InAs/GaAs quantum dots with wetting layer. Appl Opt 2012;51:4176–4185.
[20] Naumova AV, Modo M, Moore A, Murry CE, Frank JA. Clinical imaging in regenerative medicine. Nat Biotechnol 2014;32:804–818.
[21] Hong GS, Antaris AL, Dai HJ. Near-infrared fluorophores for biomedical imaging. Nature Bio Eng 2017;1:0010.
[22] Hyun H, Owens EA, Wada H, Levitz A, Park G, Park MH, et al. Cartilage-specific near-infrared fluorophores for biomedical imaging. Angew Chem Int Ed Engl 2015;54:8648–8652.
[23] Legant WR, Shao L, Grimm JB, Brown TA, Milkie DE, Avants BB, et al. High-density three-dimensional localization microscopy across large volumes. Nat Methods 2016;13:359–365.
[24] Cui W, Li J, Zhang Y, Rong H, Lu W, Jiang L. Effects of aggregation and the surface properties of gold nanoparticles on cytotoxicity and cell growth. Nanomedicine 2012;8:46–53.
[25] Kolny-Olesiak J, Weller H. Synthesis and application of colloidal CuInS2 semiconductor nanocrystals. ACS Appl Mater Interfaces 2013;5:12221–12237.
[26] Chen Y, Li S, Huang L, Pan D. Low-cost and gram-scale synthesis of water–soluble Cu–In–S/ZnS core/shell quantum dots in an electric pressure cooker. Nanoscale 2014;6:1295–1298.
[27] Shen S, Zhao L, Zhou Z, Guo L. Enhanced photocatalytic hydrogen evolution over Cu-doped $ZnIn_2S_4$ under visible light irradiation. J Phys Chem C 2008;112:16148–16155.